Neural Computing and Applications (2020) 32:12281–12294
https://doi.org/10.1007/s00521-019-04407-2

ENGINEERING APPLICATIONS OF NEURAL NETWORKS 2018

Robust anomaly identification algorithm for noisy signals: spacecraft solar panels model

Wael A. Murtada[1] · Ehab A. Omran[2]

Received: 14 December 2018 / Accepted: 30 July 2019 / Published online: 8 August 2019

Abstract
Prony method is an efficient feature extraction technique when applied to signals at noiseless environment. However, space environment is very rich with different sources of noise. Noise has a massive effect on Prony method that is noticeably degrades its performance. The objective of this research is to introduce an efficient and robust technique for fault detection and identification at noisy environment to one of the most vital subsystems in spacecraft, which is electrical power subsystem (EPS). Occurrence of anomaly in spacecraft EPS is mainly related to some parameters that are voltage, current and delivered power. This will directly affect the overall spacecraft operation and may result in partial or total mission loss. It is crucial for spacecraft onboard computer to be provided with a diagnosis task that keeps track of EPS parameters and efficiently detect and identify anomalies at different noise levels. The proposed approach is based on noisy signal energy contents. The signal energy contents are large enough compared with noise energy contents. The algorithm uses the short-time energy for noisy signals to robustly identify photovoltaic (PV) anomalies according to their causes like short circuit, open circuit and shading. The proposed approach is proved to be able to discriminate among different types of PV anomalies, and the results ensure the robustness of the proposed algorithm. This is carried out with different noise levels, with minimal task execution time and with small memory footprint. The proposed algorithm is considered to be a generic approach for noisy signal identification.

Keywords Spacecraft electrical power subsystem · Spacecraft fault detection · Spacecraft fault identification · Noisy signals feature extraction

1 Introduction

Monitoring dynamic complex systems to detect faulty behavior is always a challenge. The basic definition and concept of FDI were initially proposed by the International Federation of Automatic Control IFAC SAFEPROCESS Technical Committee [1]. Thus, many FDI techniques for space and aerospace applications had been investigated. Model-based fault diagnosis methods for aerospace systems were extensively reviewed at [2]. A deep survey and investigations for FDI strategies used in space domain were introduced at [3] that presented the importance of balancing the FDI strategy requirement such as robustness and quick identification with the limited OBC resources.

Different approaches for Prony method had been widely used for signal identification by extracting true poles and zeros from these signals, which is considered to be a signature for each signal. This scheme was proposed by researchers to be used for defining the pattern of faulty events that are occurred within monitored systems. Locating faults on transmission lines had been introduced in [4] by using Prony method to analyze traveling wave phenomenon. Another approach for differentiating faulty from non-faulty behaviors in overcurrent protection relays was developed by extracting distinct parameters for current signals utilizing Prony technique at [5]. Signal identification approaches were introduced for medical applications

✉ Wael A. Murtada
wael_murtada@narss.sci.eg

Ehab A. Omran
20110128@fue.edu.eg

[1] National Authority for Remote Sensing and Space Sciences (NARSS), Cairo, Egypt

[2] Egyptian Space Technology Center (STC/FUE), Cairo, Egypt

such as classifying electrocardiogram (ECG) and electroencephalograph (EEG) signals for detecting abnormal conditions that are based on Prony poles modeling investigated in [6–8]. Multi-Prony analysis (MPA) was introduced by [9] for estimating the critical modes of phasor measurement unit (PMU) in power measurements. However, Prony method is well known by its sensitivity to the presence of noise that limits the method ability for identification and then degrades its accuracy [10]. Several approaches were investigated for improving Prony method to tolerate the effect of noise such as extended Prony [11] that provides low accuracy and miss classifications, especially when applied to additive white Gaussian noise (AWGN). Furthermore, the modified total least squares Prony (MTLSP) method [12] is relatively a time-consuming approach and also provides a very low classification accuracy due to superimposed noise effect. Singular value decomposition technique was introduced to improve Prony performance under noise existence in [13–16]. This scheme was also very complex and time-consuming. Digital filters and frequency domain approaches were introduced in [17–19] to improve Prony method against noise effect. On the other hand, these approaches are complex and cannot be used for safety critical systems due to real-time constraints. Another technique that uses forward–backward moving windows was applied on Prony to enhance its immunity against noise as in [20, 21]. This approach was addressed for high efficiency. Unfortunately, it requires a big amount of data storage memory.

This research introduces a time domain technique that overcomes the problems that were presented in previous approaches while enhancing Prony performance to obtain high-accuracy classification capability for noise-contaminated signal. Moreover, this approach takes into consideration a spacecraft onboard computing requirements and constraints such as real-time software requirements like execution time and small memory footprint for data storage. Evaluation of the proposed approach was performed using solar panel mathematical model that was constructed based on TJ 3G28C solar cell characteristics with simulating normal and faulty conditions.

This research is organized as follows: Sect. 2 describes spacecraft EPS main components and the adopted mathematical model for the solar panels. Section 3 describes the simulation of possible anomalies for spacecraft solar panels. Section 4 illustrates Prony method as a feature extraction technique for anomalies' classification of noise-free signals. Section 5 describes the proposed algorithm that is used for tolerating the effect of noise on FDI process performance. Sections 5.1 and 5.2 describe the enhancement of Prony capability using the short-time energy concept and signal total energy contents. Section 5.3 illustrates the use of linear independency identity method for feature distinctness assessment. Section 6 includes the results and a comparative study. Finally, Sect. 7 introduces the conclusion of this research.

2 Mathematical model

EPS in spacecraft is responsible for energy generation and management. It provides enough electrical power to all spacecraft subsystems under all designed operational conditions. This is by regulating, controlling and distributing the generated power obtained from solar arrays or batteries [22]. EPS main elements and their functionality are briefly described in Figs. 1, 2.

This research focuses on the solar panel as the main generation element of power in spacecraft. Modeling of a spacecraft solar panel to satisfy power requirements of spacecraft mission depends on the characteristics of the used solar cell type. Each PV solar cell is characterized by its main electrical parameters in terms of current values at short circuit conditions, voltage values at open circuit conditions, temperature gradient effect, maximum output current, voltage and delivered power. PV solar cell performance can be described by one-diode model equivalent circuit as shown in Fig. 3. This model is commonly used to describe the output current behavior for such type of solar cells [23]. Solar cell output current is given by (1):

$$I_o = I_{ph} - I_c\left[e^{\frac{q(V_o+IR_s)}{nkt}} - 1\right] - \frac{V_o + I_0 R_s}{R_{sh}} \quad (1)$$

where I_o output current (A), V_o output voltage (V), I_{ph} PV current (A), I_c diode current (A), $R_{s,}$ series resistances (Ω), R_{sh} shunt resistances (Ω), n solar panel ideality factor, q electric charge = 1.6×10^{-19} (C), k Boltzmann constant = 1.38×10^{-23} (J/K), T and Temperature (K).

PV cell type that had been used in this research is TJ3G28C. This type is a triple-junction solar cell with electrical characteristics that are described in [24] as mentioned in Table 1.

Figure 4 shows the implementation of Simulink model for the TJ3G28C PV solar cell. This model is used to validate the one-diode PV solar cell equivalent circuit output current and power with its electrical characteristics as mentioned in Table 1. Both (P–V) and (I–V) curves were

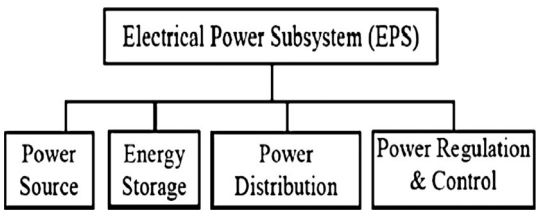

Fig. 1 Electrical power subsystem functionality

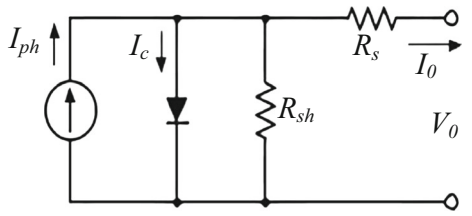

Fig. 2 Equivalent circuit of PV solar cell

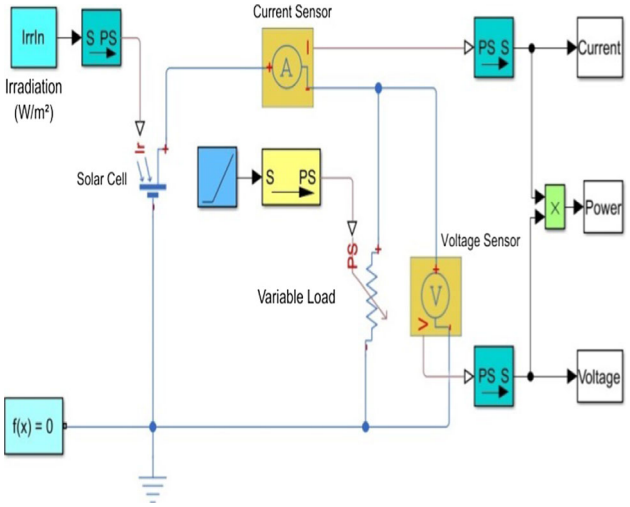

Fig. 3 Solar cell Simulink model

Table 1 TJ 3G28C technical specifications

Parameters	Value
V_{oc} (open circuit voltage)	2.667 V
I_{sc} (short circuit current)	0.506 A
V_{max} (max. voltage)	2.37 V
I_{max} (max. current)	0.487 A
P_{max} (maximum power)	1.29 W
Operating temperature T	28 °C
Voltage temperature gradient ΔVoc/ΔT	− 0.006 V
Current temperature gradient ΔIsc/ΔT	0.00032A

estimated based on the data sheet values at standard test conditions (STC).

Where: solar irradiation I_{rr} = 1367 w/m^2; diode current $I_c = 2.3 \times 10^{-13}$ A; series resistances R_s= 0.005 Ω; shunt resistances R_{sh}= 360 Ω; solar panel ideality factor n = 1.3.

Figures 4 and 5 illustrate the model simulation for TJ3G28C solar cell output current and power characteristics. From these figures, it is obvious that the solar cell model successfully achieves the required data sheet electrical characteristics.

The second step of modeling is to use TJ3G28C solar cell to design a solar panel. This solar panel can supply a

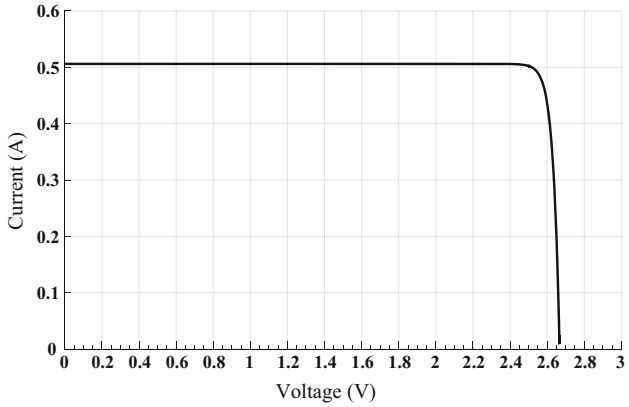

Fig. 4 Solar cell ($I-V$) characteristics

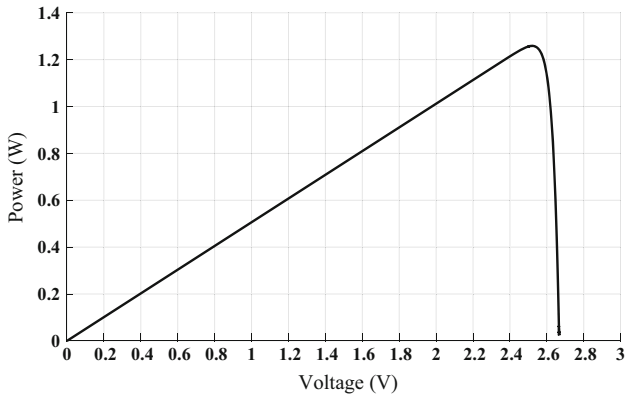

Fig. 5 Solar cell (P–V) characteristics

bus voltage, load current and satisfying power budget that is required for spacecraft mission. Proposed case study requirements are shown in Table 2.

Based on requirements that are mentioned in Table 2, the solar panel Simulink model was designed to include 40 parallel strings. Each string consists of 17 series solar cells and for more protection and isolation capability, the 40 strings were divided into eight generator modules. Each

Table 2 Spacecraft electrical power requirements

Parameters	Value
Nominal voltage (V)	27–32
Supply voltage (V)	42–45
Maximum power (W)	1200
Nominal power (W)	1000
Max load current (A)	24–26
Temperature range (°C)	− 20 to 75
Thermal and connection voltage drop (%)	27%
Thermal and connection current losses (%)	30%

generator module contains five parallel strings and is protected by a series blocking diode as shown in Figs. 6 and 7.

Figures 8 and 9 illustrate the solar panel load current, bus voltage and delivered power that matches spacecraft electrical power system requirements. These parameters represent the basic constraints that define normal operation of spacecraft electrical power system. The aim of the proposed FDI technique is to detect and identify anomalies that will occur in solar panels in terms of current, voltage and power.

3 Solar panel anomalies simulation

Spacecraft solar panel anomalies are typically referred to some basic causes [25, 26]. Most of these anomalies are caused by open circuit, short circuit and partial shading. This is due to spacecraft miss orientation from sun angle that decreases the maximum irradiation and affects charging of batteries.

The main categories of these anomalies are divided into subclasses for each PV generator module as shown in Fig. 10 and Table 3. Solar panel mathematical model is used for simulating all possible types of these anomalies. Figures 11 and 12 present (*I–V*), (*P–V*) characteristics for ten subclasses of anomalies in addition to normal operation behavior.

The above figures introduce the impact of PV anomalies for voltage, current and power signals. Furthermore, open circuit and shading anomalies result in drop of solar panel maximum output current. However, short circuit anomaly causes a noticeable drop of the maximum voltage. In general, all types of PV anomalies will cause a drop at maximum delivered power. Monitoring of power signal amplitude is required for anomaly detection, but it is not enough to identify the cause and type of anomaly. The generated time-varying power signal varies in amplitude regardless of anomaly reason that had been caused by either voltage or current drop. Therefore, it is required for the fault classifier to be trained with distinct signal features to differentiate among specific PV anomalies. The efficient

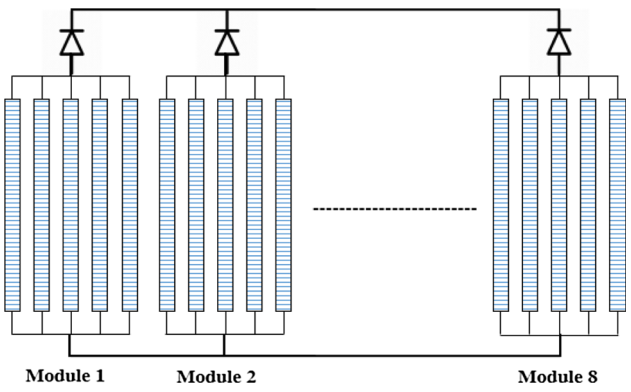

Fig. 6 Solar panel configuration

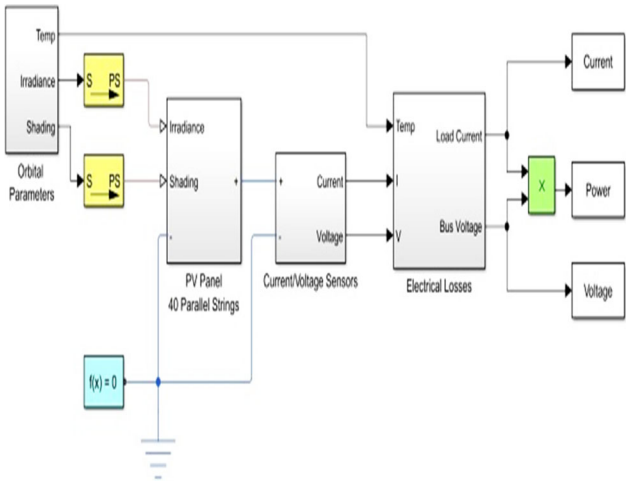

Fig. 7 Solar panel model

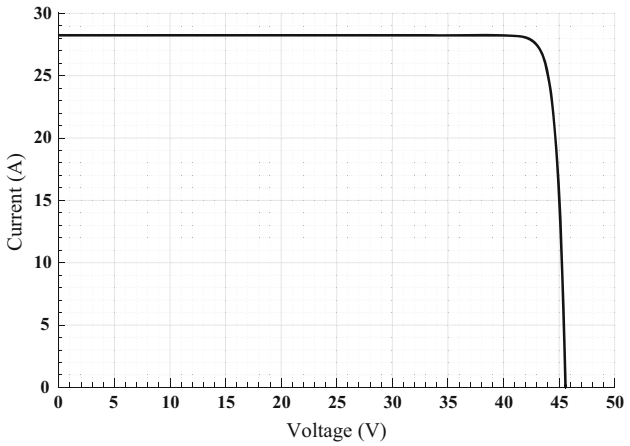

Fig. 8 Solar panel (I–V) characteristics

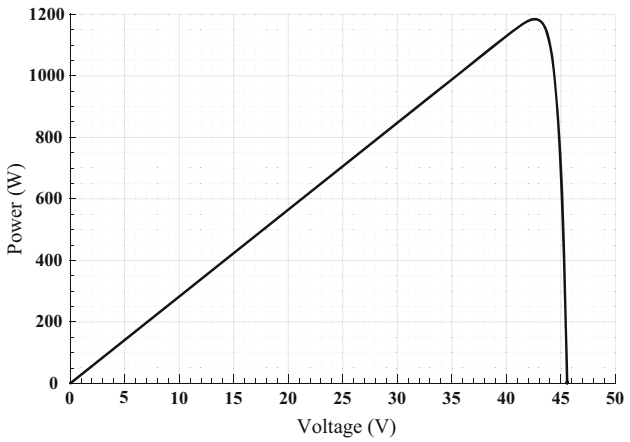

Fig. 9 Solar panel (P–V) characteristics

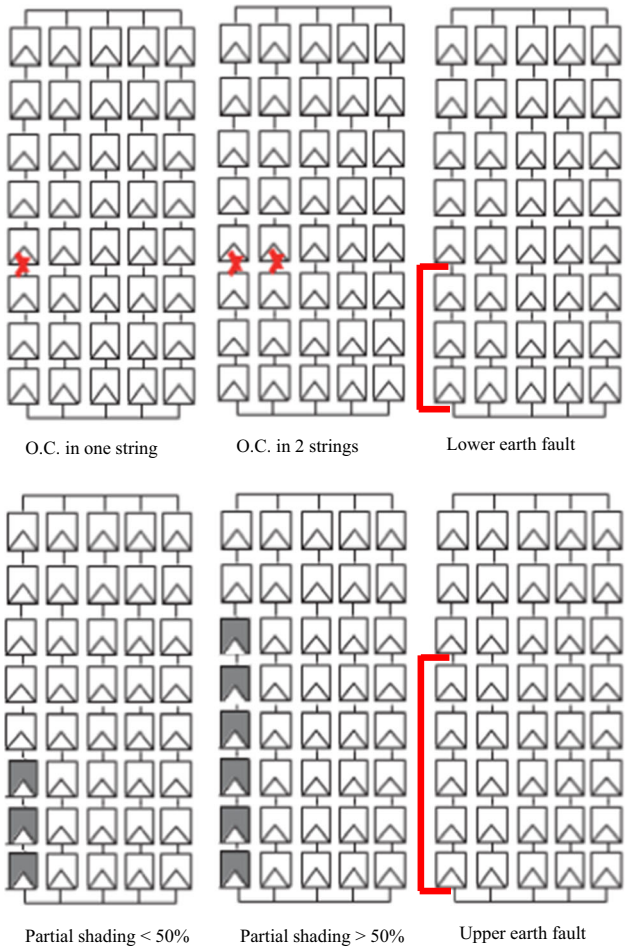

Fig. 10 Causes of solar panel anomalies

way is to apply a suitable feature extraction technique that produces distinct features for each anomaly type. The proposed feature extraction technique for this time domain signal is based on Prony approximation. Furthermore, Prony method is proved to have an effective performance for analogous applications and studies as introduced in [27].

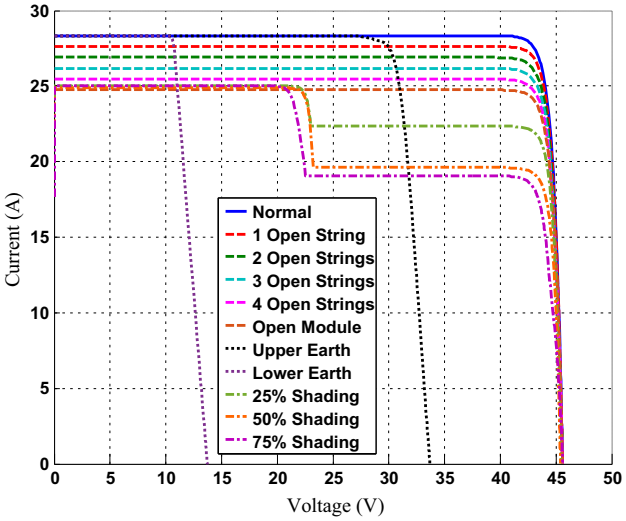

Fig. 11 Solar panel anomalies (I–V) characteristics

4 Anomaly classification

The success of spacecraft mission is highly dependent on solar panel reliability. Moreover, reliability guarantees the proper functionality of all spacecraft subsystems. Furthermore, when the solar panels cannot deliver the required power, the spacecraft should reduce the active hardware configuration to the extent that utilizes only the available power. This leads to limit the spacecraft functionalities or causes mission failure. One of the most vital tasks of OBC software is real-time monitoring for the generated solar panel power signal. This task is crucial in order to detect and identify PV transducer anomalies.

Figure 13 presents the modeled solar panel output power versus time for each case of anomalies as well as the solar panel nominal operating conditions. Moreover, normal solar panel behavior is satisfied by applying the operating parameters and conditions as listed in Table 2.

Table 3 Solar panel anomalies' subclasses per each generator module

Anomaly ID	Anomaly type	Anomaly code	Anomaly subclass cause per module
0	None	N	Normal operation
1	Open circuit	A1	Open circuit in 1 string
2		A2	Open circuit in 2 strings
3		A3	Open circuit in 3 strings
4		A4	Open circuit in 4 strings
5		A5	Open circuit module
6	Short circuit	B1	Upper earth fault $> 50\%$
7		B2	Lower earth fault $< 50\%$
8	Shading	C1	25% partial shading
9		C2	50% partial shading
10		C3	75% partial shading

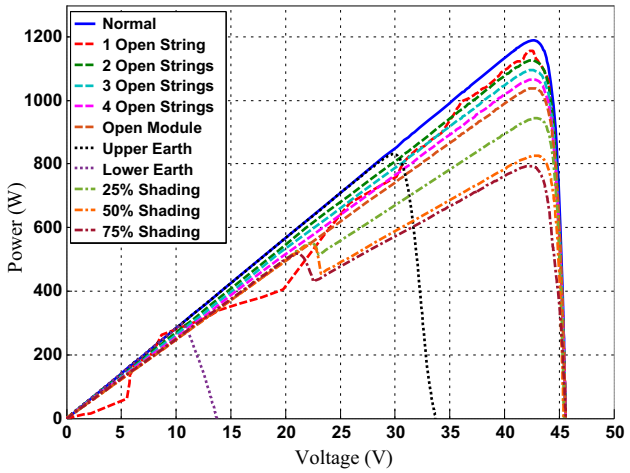

Fig. 12 Solar panel anomalies (P–V) characteristics

The power–time curve shown in Fig. 13 is obtained by multiplying the modeled output current and voltage values every 1 ms and then stored to OBC memory. Furthermore, the stored data are monitored and processed each time interval of 500 ms. The selection criteria for the time interval depends mainly on the OBC operating system scheduler that is designed to perform the FDI task for EPS subsystem each 500 ms.

A recent research [27] provides a generic and efficient FDI technique for spacecraft subsystem anomalies. This technique is based on Prony approximation to extract distinct signal features for each anomaly. Prony method provides a finite set of poles and zeros that represent the signal signature. This technique can be applied to power signals presented in Fig. 13 assuming noise-free environment. It produces 100% accuracy for classifying all types of PV anomalies into different categories as depicted in Fig. 14.

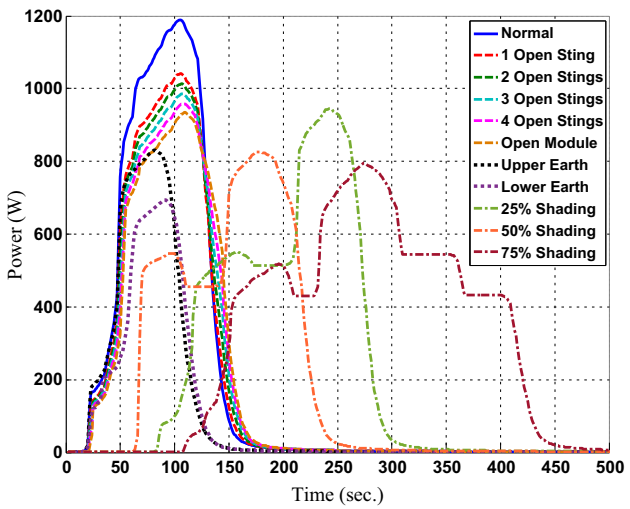

Fig. 13 Modeled solar panel power versus time signals

However, the harsh space environment imposes different types of noise with different noise levels. Moreover, noise appears as a fluctuation in power signals that are generated by solar panels and had been caused by DC-to-DC converters switching in addition to any other space noise sources. This noise can be modeled by AWGN *s(t)* with several amplitudes and different frequencies. The noisy signals can be represented by (2) as follows:

$$y_{\mathrm{n}}(t) = w_{\mathrm{f}}(t) + s(t) \tag{2}$$

where $y_{\mathrm{n}}(t)$ noise-contaminated signal; $w_{\mathrm{f}}(t)$ noise-free signal; $s(t)$ AWGN signal.

Figure 15 presents the normal power signals after adding AWGN with relative amplitude levels of 10%, 20% and 30% of signal peak amplitude. This is equivalent to SNR of 20 dB, 13.9 dB and 10.4 dB, respectively. However, negative portion of power signal amplitude is due to addition of negative values for random noise amplitudes.

5 Proposed noisy signal identification approach

Applying Prony method for extracting distinct signal features is efficient for non-noisy signals as in [27]. But in case of noise-contaminated signals, it results in low classification accuracy, because Prony method feature extraction mechanism is significantly affected by noise [28]. Noise will always produce irrelevant features in case of using Prony method directly without enhancement by any further approaches.

Furthermore, applying any type of filters for noise removal before extracting Prony signal features results in miss classification or very low classification accuracy. This is due to signal distortion that is generated by imposing

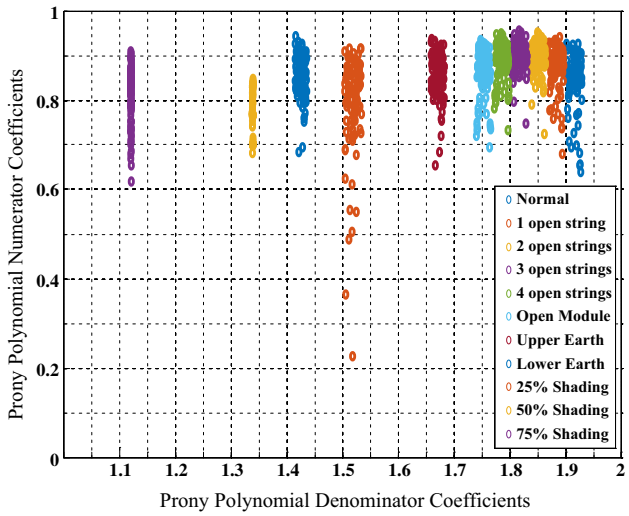

Fig. 14 Prony features for normal and faulty PV power signals

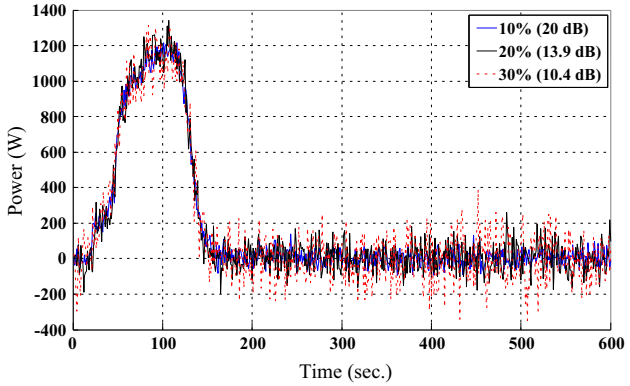

Fig. 15 Normal operating conditions for solar panel power signals at different noise amplitude levels

random AWGN patterns with different amplitude levels to the original signal. This will affect classification process in a manner; that is, the generated patterns will be different at each time that random AWGN is imposed. The proposed approach, as described in Fig. 15, is based on energy contents of noisy power signals. It is basically based on the principal that energy contents of clean signal are dominant and greater than energy of noise signal. Furthermore, the proposed approach enables transformation into energy versus time domain to identify nominal and different faulty power signals with different noise levels. To get a discriminant features from the generated faulty power signals, it is appropriate to find distinct parameters to construct such features. Moreover, noisy signal variance, total energy contents of noisy power signals and Prony poles are preferred to be feature vector parameters as a discriminant factor. Using STE approach will transfer the analysis to energy–time domain. Therefore, feature extraction process should be applied there in a manner that facilitates signal identification.

5.1 Prony feature extraction for STE signals

STE is defined at [29] as the energy contents in a short-time segment of the signal. STE had been mainly used for voice recognition, discrimination and voice activity detection applications as introduced in [30, 31]. Short-time energy introduces an efficient way for noisy signal identification, because noise energy is small compared with clean signal energy. Thus, original signal energy is dominant.

On the other hand, this proposed method mitigates Prony sensitivity against large variations in signal pattern. Signal pattern distortion is caused by additive noise amplitudes that impose positive or negative values of noise levels. When the input noisy signal $y(t)$ is segmented to "N" short segments with equidistant intervals of length "L", then the short-time energy STE_i for each segment is equal to the sum of the square short segment samples' values that is represented by (3) as follows: $\forall\, i = 1, 2, \ldots N$ segments, $\exists \mathrm{STE}_i \ni$

$$\mathrm{STE}_i = \sum_{j=1}^{L} y_j(t)^2 \tag{3}$$

where STE short-time energy; y sample value; L segment length; N number of equidistant segments; i segment index; j sample index.

Hence, the short-time energy for all N segments STE will be defined in matrix form as (4):

$$\mathrm{STE} = [\,\mathrm{STE}_1 \quad \mathrm{STE}_2 \ldots \quad \mathrm{STE}_N\,] \tag{4}$$

Due to harsh space environment, it is proposed to transform PV transducers' power signals into energy signals. Furthermore, STE of each segment represents a point in time. Thus, the generated energy for normal and faulty signals shall be identified well. Thanks for Prony feature extraction that helps to produce efficient signal's signature as in [27]. The proposed algorithm is shown in Fig. 16.

Signal poles and zeros can be estimated by applying Prony method of orders (K, Q) for energy signal $E(t)$ as in (5a), (5b):

$$S(z) = \frac{B(z)}{A(z)} = \frac{\sum_{i=0}^{Q-1} b_i z^{-i}}{1 + \sum_{j=1}^{K-1} a_j z^{-i}} \tag{5a}$$

$$S(z) = \frac{b_0 + b_1 z^{-1} + \cdots + b_{Q-1} z^{-(Q-1)}}{1 + a_1 z^{-1} + \cdots + a_{k-1} z^{-(K-1)}} \tag{5b}$$

where $S(z)$ signal Z-transform, $B(z)$ numerator polynomial, $A(z)$ denominator polynomial, b_i numerator polynomial coefficients, $i = 0 \ldots Q-1$, a_j Denominator Polynomial coefficients, $j = 1 \ldots K-1$, K, Q Prony Approximation orders for poles and zeros, respectively.

Poles vector "P" is one of the features that will be used in signal identification. It can be expressed as all poles polynomial $A(z)$ according to Eqs. (6), (7)

$$A(z) = 1 + a_1 z^{-1} + a_2 z^{-2} + \cdots + a_{k-1} z^{-(K-1)} \tag{6}$$

$$P = [\,a_1 \quad a_2 \ldots \quad a_{K-1}\,]^T \tag{7}$$

The main advantage of using Prony poles instead of taking all short-time energy values, as a signal features, is to reduce a signal feature vector size.

Thus, this is useful for embedded systems that have a limited memory size. This feature extraction criterion is acting as a dimensionality reduction mechanism with a reduction ratio of $\eta, where (K - 1 \ll N)$ as shown in (8).

$$\eta = \frac{N - (K-1)}{N}\,\% \tag{8}$$

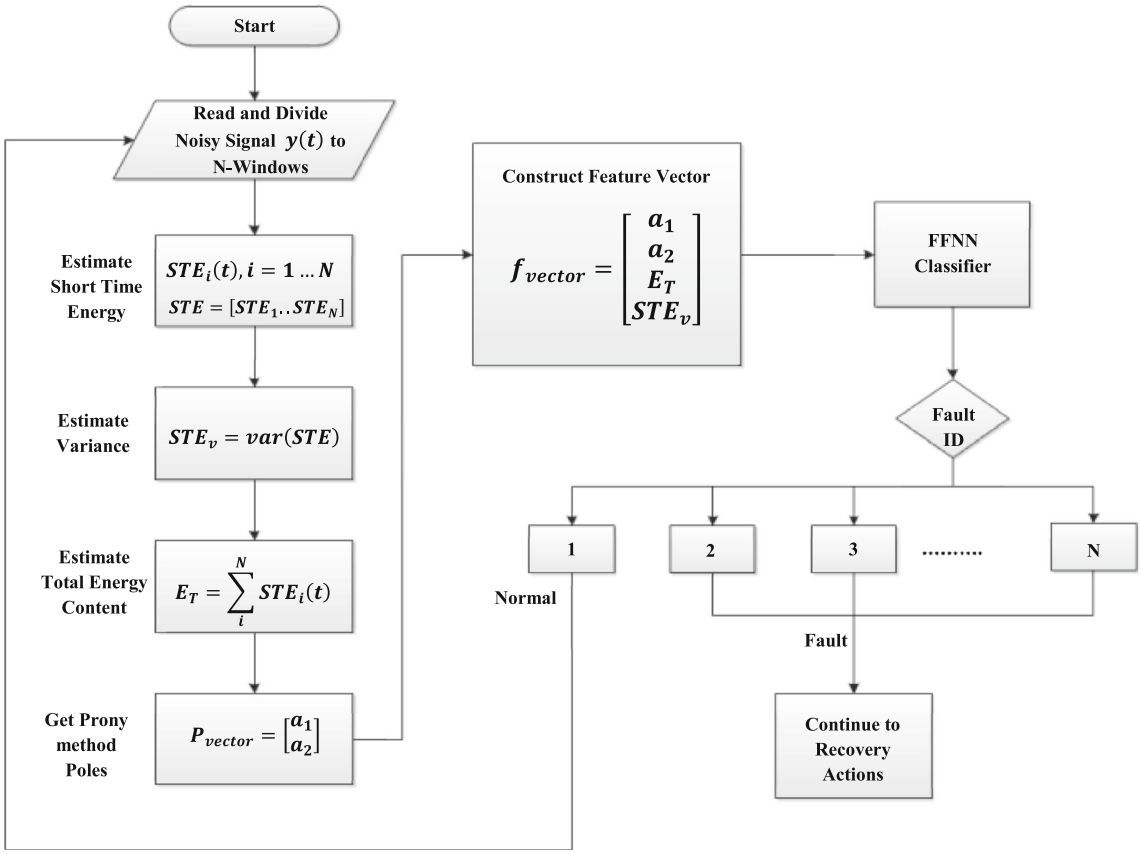

Fig. 16 Proposed algorithm flowchart

where η is dimensionality reduction ratio, N represents the number of equidistant signal segments and K is the number of Prony poles.

For example, applying Prony of the third order for short-time energy signal over 100 segments produces a feature vector "P" that contains only two signal poles in the form $[a_1 a_2]^T$, which significantly reduces the stored dataset at onboard limited memory by (98%). This proposed method will help to satisfy memory limitation requirement in a manner that conform spacecraft onboard computer requirements.

Figure 17 presents STE with $N = 60$ segments for normal PV power signal response, open circuit, short circuit and shading anomalies at different additive noise levels of 10%, 20% and 30%. Noise-level values are equivalent to SNR = 20 dB, 13.9 dB and 10.4 dB, respectively. As shown in Fig. 17, it is noticeable that the STE values were slightly affected by noise amplitude levels.

On the other hand, selecting Prony order is crucial to minimize signal feature vector size. This will affect the OBC memory footprint. In order to determine optimal Prony poles order from Fig. 17 patterns, it shall be suitable to select the third-order Prony approximation. More than third order will be redundant and then enlarge signal signature memory footprint. Furthermore, signal poles signature of denominator polynomial will lead to enough representation of these types of signals. Insertion for zeros of the numerator polynomial will lead to non-feasible feature representation. This is because the zeros approximately have similar values. Prony poles features are not enough to represent signal signature. This is due to similarity of these features with others for other anomaly signals. As a result, interference of anomalies features will occur as shown in Fig. 18. They become no more distinct features that lead to misclassification of different signals, hence decreasing the efficiency of the FDI technique. In order to discriminate among anomalies and normal behavior signals, it shall be a need for other feature elements in a manner to distinguish each signal. For this reason, it is suitable to define other feature element like STE signal variance as in next subsection.

5.2 Variance of short-time energy signal and total energy contents

The second element of feature vector is the variance of STE values. Variance is the expectation of the squared deviation of random values from their mean. It is a

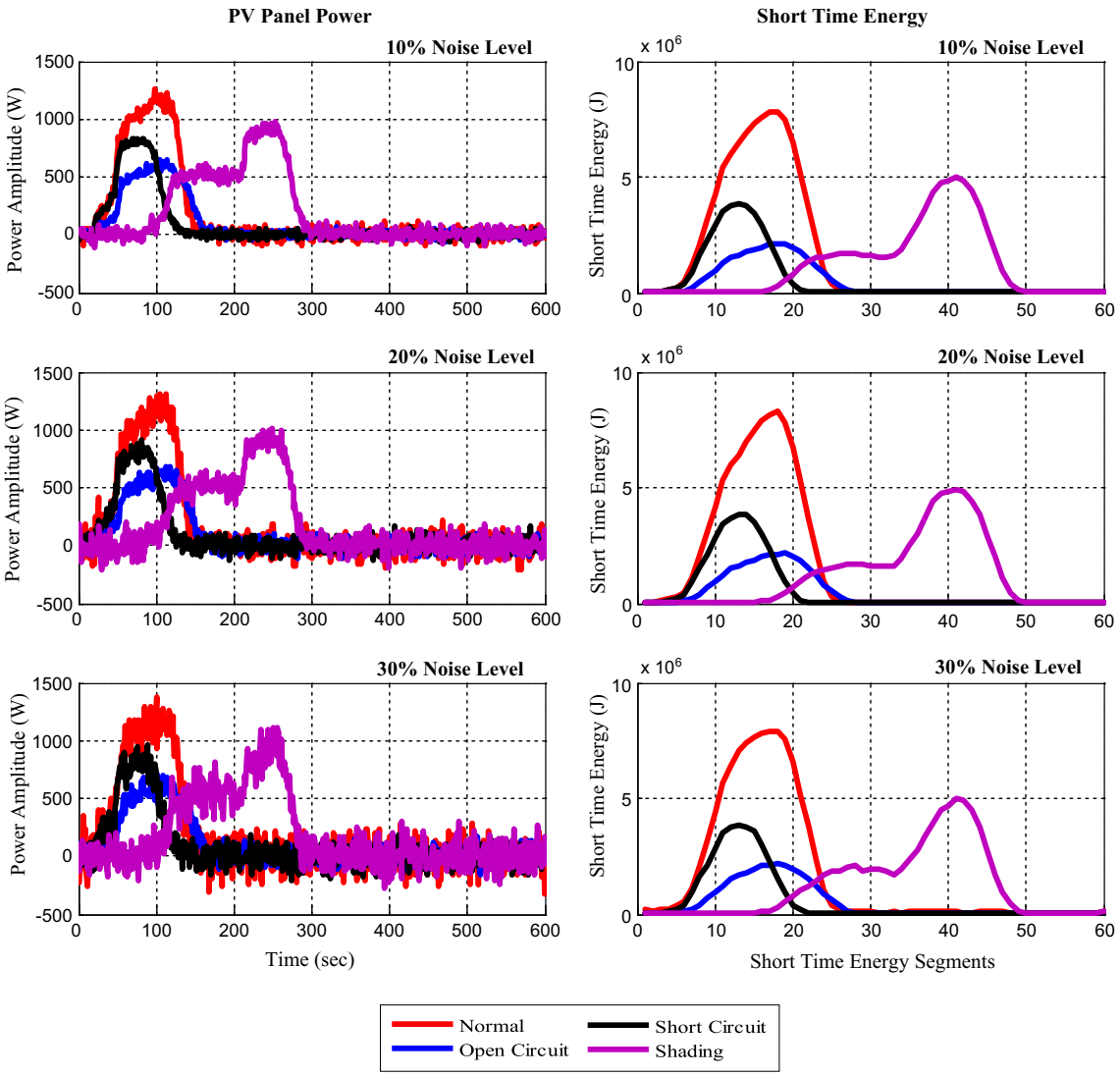

Fig. 17 Short-time energy for normal signal, open circuit, short circuit and shading anomaly signals at different noise levels

statistical measure for how far these random values are spread out from their arithmetic mean [32]. In this case study, it is proposed to use this measure in a manner to study the dispersion of STE values at different additive noise levels from their mean value. Thus, the variance value at signal feature vector is then indicative and produces a distinctive feature.

Variance of short-time energy can be defined by (9) as follows:

$$\mathrm{STE}_v = \frac{1}{N}\sum_{i=1}^{N}\left(\mathrm{STE}_i - \hat{\mathrm{STE}}\right)^2, \tag{9}$$

where STE_v variance of STE values; STE_i magnitude of STE values for each segment; $\hat{\mathrm{STE}}$ mean of STE values; N number of STE values.

In order to characterize the generated PV power signal, the total energy contents is crucial to identify such normal and anomaly signals.

Nevertheless, by means of area under the STE versus time curves, the total energy contents $\mathrm{E_T}$ can be defined for specific measured time window $T = N \times L$ as in (10)

$$E_T = \int_0^T \mathrm{STE}_i \mathrm{d}t \tag{10}$$

To evaluate E_T, it is proposed to use trapezoidal integration for simplicity. Figure 19 introduces STE variance for normal-type signal at noise levels 1% to 30% that are equivalent to SNR = 20 dB to 10.4 dB, respectively. Figure 20 introduces total energy contents for normal-type signal at noise levels 1% to 30% that are equivalent to SNR = 20 dB to 10.4 dB, respectively.

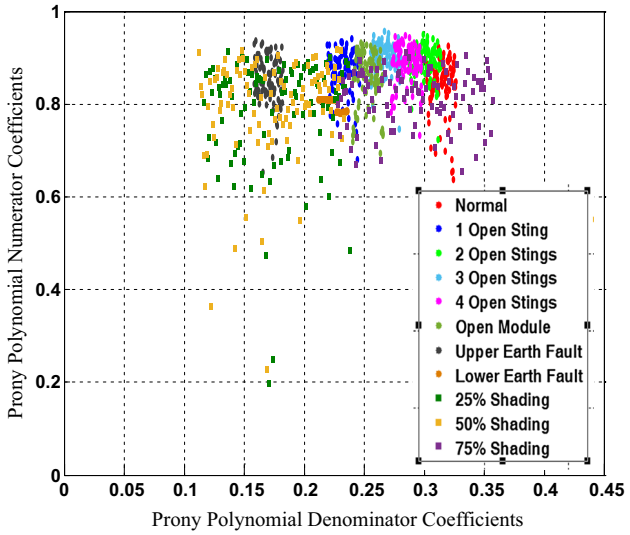

Fig. 18 Prony features for normal and faulty PV power signals in the presence of noise

5.3 Features distinctness assessment

Signal features distinctness is a catalyst for any feed-forward neural network (FFNN) to get an efficient classification performance. Therefore, FFNN is trained by means of distinct features and that such distinctness is assessed and tested by the linearly independent vectors identity (11) as in [33]:

$$a_1 f_1 + a_2 f_2 + \ldots + a_n f_n = 0 \tag{11}$$

where n number of signals; $f_{1..n}$ signals' feature vector; $a_{1..n}$ scalar coefficients.

In this case study, the number of signals (n) = 11 and the feature vector are formed by combining the proposed four feature elements as in (12)

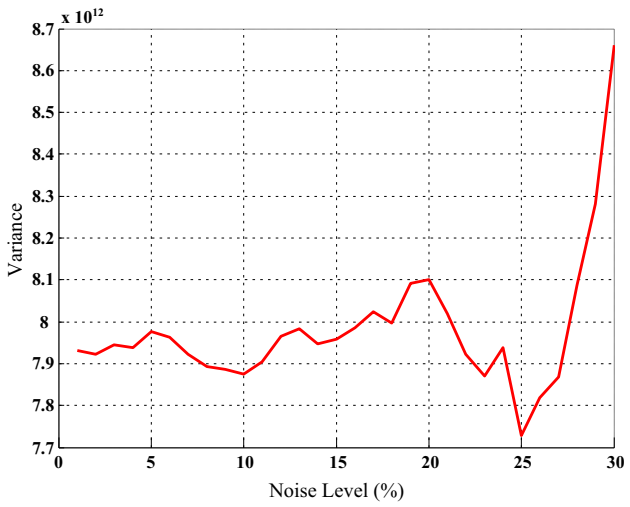

Fig. 19 STE variance for normal signal at different noise levels

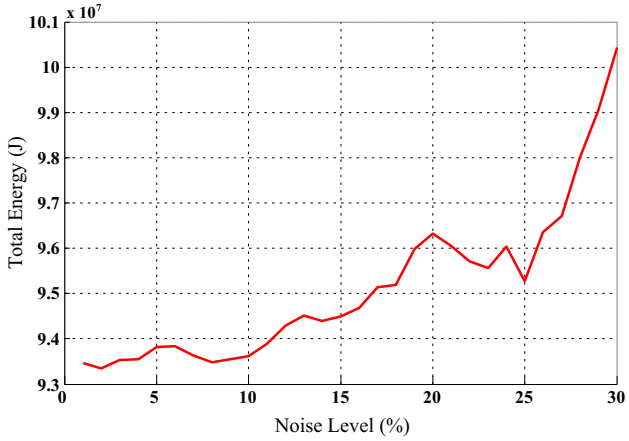

Fig. 20 Total energy for normal signal at different noise levels

$$f_i = [P_1 \quad P_2 \quad \mathrm{STE}_v \quad E_T]_i^T, \quad i = 1 \ldots n \tag{12}$$

where $P_1 P_2$ signal poles; STE_v variance of STE signal; E_T signal total energy contents.

Checking for linear independency is performed by determining the values of scalar coefficients such that when $a_1, a_2 \ldots, a_n = 0$, then all feature vectors are linearly independent and then distinct. While a nonzero value for, at least, one of these coefficients indicates the existence of linear dependency relationship among features and leads to non-fully distinctive. The distinct features enable FFNN to be trained efficiently and result in high-performance classification. Furthermore, thanks for linear independency identity (11) that helps to prove that all measured power signals' features are linearly independent and then distinct. The overall dataset is formed by generating 100 feature vectors for each signal type using the mathematical model by varying the simulated irradiation inputs from 1000 to 1300 W/m^2 with a step of 3 W/m^2 such that the dataset will form a matrix of 400 × 11 elements as in (13)

$$\begin{bmatrix} \begin{bmatrix} P_1 \\ P_2 \\ STE_v \\ E_T \end{bmatrix}_{1_1} & \begin{bmatrix} P_1 \\ P_2 \\ STE_v \\ E_T \end{bmatrix}_{1_2} & \cdots & \begin{bmatrix} P_1 \\ P_2 \\ STE_v \\ E_T \end{bmatrix}_{1_{11}} \\ \begin{bmatrix} P_1 \\ P_2 \\ STE_v \\ E_T \end{bmatrix}_{2_1} & \begin{bmatrix} P_1 \\ P_2 \\ STE_v \\ E_T \end{bmatrix}_{2_2} & \cdots & \begin{bmatrix} P_1 \\ P_2 \\ STE_v \\ E_T \end{bmatrix}_{2_{111}} \\ \vdots & \vdots & \cdots & \vdots \\ \begin{bmatrix} P_1 \\ P_2 \\ STE_v \\ E_T \end{bmatrix}_{100_1} & \begin{bmatrix} P_1 \\ P_2 \\ STE_v \\ E_T \end{bmatrix}_{100_1} & \cdots & \begin{bmatrix} P_1 \\ P_2 \\ STE_v \\ E_T \end{bmatrix}_{100_{11}} \end{bmatrix} \tag{13}$$

6 Results

The proposed FDI strategy architecture is mainly divided into two stages. The first stage is an offline processing that prepares the PV signals' feature datasets for normal and faulty signals. Moreover, this stage is carried out only once at ground station using the proposed mathematical model. Therefore, the obtained feature vectors will be stored at the OBC memory before spacecraft launching. The second stage is the real-time feature extraction and identification processes. This stage will be executed at spacecraft OBC by a centralized FDI software task, which is at the top layer of the mission software. The FDI task is based on the proposed algorithm as shown in Fig. 16 that will perform feature extraction and then fault classification with real-time constraints.

Feature vectors are obtained from a dataset of 100 signals that were provided by PV mathematical model to train a neural network classifier that is based on FFNN type with a single hidden layer, 11 input neurons and 21 hidden neurons.

Training was achieved for each type of anomalies in addition to normal case power signal using noise-contaminated signals with noise levels (1% up to 30%). Figure 21 and Table 4 prove that the proposed approach introduces (100%) classification accuracy at noise amplitude levels up to 30%.

Moreover, it is found that fault identification task of solar panel single anomaly has an average execution time of 10 ms at onboard target processor MIPS R3000. Therefore, average task execution time is found to be suitable for typical spacecraft onboard platforms. This is because most of the spacecraft onboard computers have an overall average computational time frame about 200 ms [34]. On the other hand, regarding onboard resources limitations of spacecraft, the proposed technique is considered to be a superior solution for such a problem. Thus, proposed technique provides low memory footprint due to the small number of extracted features instead of original signal features. Moreover, it, respectively, speeds up execution time and increases onboard performance.

The proposed approach is compared to other FDI techniques, such as model-based techniques in [35–37] that used Hidden Markov Model (HMM) or Qualitative Event-based Diagnosis (QED) that focuses only on detecting the faulty state without deep identification of anomaly nature. The proposed technique was also compared to other detection and identification techniques as shown Table 5, such as large-scale Bayesian technique in [38] and feature extraction methods such as principal component analysis with support vector machine (PCA-SVM) as in [39]. Furthermore, recent approaches that use PCA and weighted proximal support vector machine (WSVM) as in [40]. Furthermore, the proposed algorithm introduced a higher accuracy for anomaly classification in noiseless and noisy environments compared with presented technique in [16] that produces 98% classification accuracy using SVD-TLS Prony, or in [41] that provides 97% classification accuracy for both noiseless and noisy environments using STE-SVD feature extraction technique and multi-layer SVM classifier. The comparative study results that are introduced in Table 5 shows the supremacy of the proposed approach for fault classification accuracy over other recent techniques that were applied at noise levels up to 30%. Therefore, this

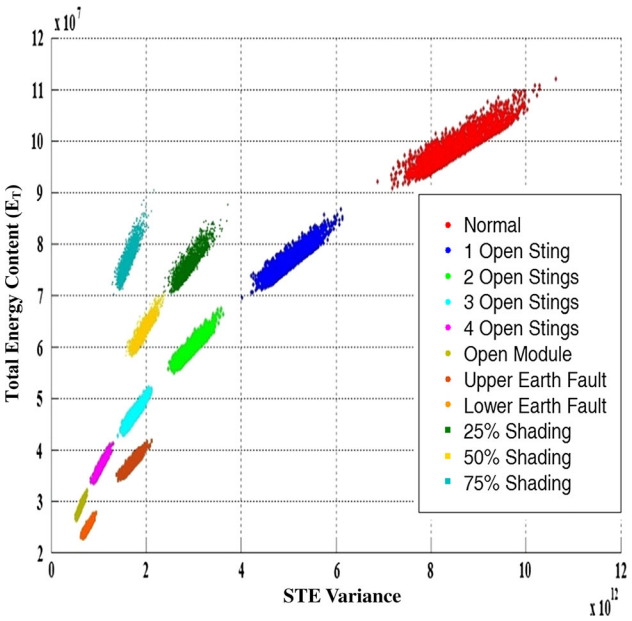

Fig. 21 Features representation for normal and anomaly signals at noise levels (1% up to 30%)

Table 4 Classification results

Fault ID	% Accuracy at noise levels					
	Clean	10%	20%	30%	40%	50%
N	100	100	100	100	100	98
A1	100	100	100	100	91	84
A2	100	100	100	100	92	85
A3	100	100	100	100	89	80
A4	100	100	100	100	89	81
A5	100	100	100	100	94	85
B1	100	100	100	100	97	86
B2	100	100	100	100	96	85
C1	100	100	100	100	84	78
C2	100	100	100	100	80	76
C3	100	100	100	100	82	74
Total	100	100	100	100	90.3	75.9

technique increases classifier robustness against noise for noise amplitude levels up to 30% of signal amplitude. The proposed approach is compared as well to the recent state-of-the-art strategies that are used for detecting the same kind of faults in PV arrays such as [42–44], whereas different improved KNN-based monitoring schemes were adopted for detecting faults in PV systems.

The comparison of results showed that the maximum accuracy obtained using these schemes is 99.4% for short circuit faults and 98.2% for shading faults, while resulted accuracy for the proposed approach is 100% for all types of these faults. This higher accuracy is achieved at the expense of higher average time required for fault detection when compared to the Kalman filter-based approach in [45] that is used for detection of series arc fault in photovoltaic systems. Optimization of factors affecting the performance of FDI process such as accuracy, time and memory footprint tends to make the proposed approach the most appropriate one for these types of space applications.

The noticeable supremacy of the proposed approach over above-mentioned techniques is the research interest with noise-contaminated environment. The proposed scheme depends mainly on the innovative selected features for the classifier training. Using noise filters was known by their complexity and tendency to distort the original signal. Thus, the proposed identification signal features are at energy–time domain that produce an approximately fixed pattern for each signal even when contains random noise amplitudes. Dealing with noisy signals from this point of view is the main objective for developing a robust, innovative and accurate FDI scheme.

7 Conclusion

This research presents a robust, generalized and efficient FDI technique using STE-Prony scheme for extracting distinct features from noisy signals that are related to spacecraft solar panel anomalies. The proposed scheme is combined with FFNN classifier that produces a robust FDI technique for classification over other noise-sensitive techniques by 100% accuracy for identifying all types of anomalies in noisy environment at noise amplitude levels up to 30% of signal amplitude. The proposed approach complies with spacecraft onboard processing time and memory limitation constraints as it provides low average execution time and small memory footprint in terms of reduced size of selected features. Furthermore, the proposed scheme is proved to be perceptibly superior when compared to contemporary techniques that employ feature extraction approaches such as KPCA and hybrid approaches such as PCA-WSVM or PCA-SVM as shown in Table 5. Moreover, this technique provides a very high accuracy compared to other STE-based techniques for noisy and noiseless environment such as SVD-TLS Prony and STE-SVD as listed in Table 5.

It is difficult to detect and identify signals at noise-contaminated environment. Most of FDI research activities are interesting with solar panels faults like renewable

Table 5 Comparative study of fault detection and classification accuracies at noise-free and noise levels up to 30%

Environment	FDI Technique	Detection accuracy (%)	Classification accuracy (%)
Noise-free	QED-PC	98	NA
	QED	98.7	NA
	HMM	100	NA
	Bayesian	100	75
	KNN	100	81
	PCA and SVM	100	89
	KPCA	100	90
	PCA and WPSVM	100	93
	Prony and FFNN [27]	100	100
Noise levels (up to 30%)			
	Prony and FFNN [27]	92	80
	STE-SVD and SVM	100	97
	SVD-TLS Prony	100	98
	STE-Prony and FFNN	100	100

The proposed scheme is tested using FFNN classifier by applying different cases of anomalies inside the training range by varying the simulated irradiation input step by 0.5 W/m^2 for the mathematical model from 0.5 to 2.5 W/m^2. Therefore, the generated datasets are used for testing and validating the proposed algorithm. All results introduce (100%) classification accuracy within the permissible time frame.

energy applications. Thus, most of the signal identification approaches that work at noisy environment use preprocessing facilities, such as filters or statistical approaches, before identification. However, all types of filters distort signal patterns and it is difficult to retrieve original signal pattern to be identified. Therefore, mapping PV noisy signals to energy domain represents the best assumption in a manner that conserve signals' patterns. On the other hand, the most innovative part of the proposed scheme is the signal features. The feature vector is accurately describing the signal in a manner that fully distinguishes among all types of faults and normal behavior. Thus, the identification process becomes possible, innovative and robust using this proposed approach.

Compliance with ethical standards

Conflict of interest The authors declare that they have no conflict of interest.

References

1. Isermann R, Balle P (1997) Trends in the application of model-based fault detection and diagnosis of technical processes. Control Eng Pract 5(5):709–719. https://doi.org/10.1016/S0967-0661(97)00053-1
2. Marzat J, Piet-Lahanier H, Damongeot F, Walter E (2012) Model-based fault diagnosis for aerospace systems: a survey. J Aerosp Eng 226(10):1329–1360. https://doi.org/10.1177/0954410011421717
3. Tipaldi M, Bruenjes B (2015) Survey on fault detection, isolation, and recovery strategies in the space domain. J Aerosp Inf Syst 12(2):235–256. https://doi.org/10.2514/1.I010307
4. Tawfik M, Morcos M (2001) ANN-based techniques for estimating fault location on transmission lines using Prony method. IEEE Trans Power Deliv 16(2):219–224. https://doi.org/10.1109/61.915486
5. Jawad F, Saeed L (2007) Prony-based optimal bayes fault classification of overcurrent protection. IEEE Trans Power Deliv 22(3):1326–1334. https://doi.org/10.1109/TPWRD.2006.886794
6. Moustafa A, Yasser M, Mohamed E, Fatma M (2009) Electrocardiogram signals identification for cardiac arrhythmias using Prony's method and neural network. In: 31st IEEE international conference on of the EMBS, USA, pp 1893–1896. https://doi.org/10.1109/iembs.2009.5333035
7. Moustafa A, Yasser M, Mohamed E, Fatma M (2010) A novel method for ecg signal discrimination of cardiac arrhythmias based on pade's approximation technique. In: 27th national radio science, Egypt, pp 1–9
8. Osama A, Ayman E, Fatma E (2014) Parametric modeling of ICTAL epilepsy EEG signal using Prony method. Int J Comput Sci Softw Eng 3(1):86–89
9. Camilo A et al (2016) Prony-based on-line oscillation detection with real PMU information. Int IEEE Conf Robot Autom, pp 1–5. https://doi.org/10.1109/ccra.2016.7811401
10. Ramdas K, Donald W, Louis L (1984) A Prony method for noisy data: choosing the signal components and selecting the order in exponential signal models. IEEE Proc 72(2):230–233. https://doi.org/10.1109/PROC.1984.12849
11. Gómez R, Carrión M (1986) Extended Prony method applied to noisy data. Electron Lett 22(11):613–614. https://doi.org/10.1049/el:19860417
12. William M, Ching J (1994) A modified TLS-Prony method using data decimation. IEEE Trans Signal Process 42(9):2292–2303. https://doi.org/10.1109/78.317852
13. William M, Ching J, Randolph L (1991) Statistical analysis of SVD-Prony techniques. In: International 25th conference on signals, systems and computers, USA, pp 232–236. https://doi.org/10.1109/acssc.1991.186447
14. Monique P, Roberto C, Martha V (1993) Modeling and classification of biological signals using least-squares Prony-SVD AR modeling. In: 36th midwest symposium on circuits and systems, USA, pp 445–448. https://doi.org/10.1109/mwscas.1993.342992
15. Mazzola M, Younan N, Soundararajan R, Saddow S (2014) Application of the singular valve decomposition–Prony method for analyzing deep-level transient spectroscopy capacitance transients. Rev Sci Instrum 69(6):2459–2463. https://doi.org/10.1063/1.1148974
16. Liu D, Hu W, Chen Z (2008) SVD-TLS extending Prony algorithm for extracting UWB radar target feature. J Syst Eng Electron 19(2):286–291. https://doi.org/10.1016/S1004-4132(08)60080-8
17. Rodney J, Marianela L, Marco P (2014) Improving the performance of the Prony method using a wavelet domain filter for MRI denoising. Comput Math Methods Med 2014:1–10. https://doi.org/10.1155/2014/810680
18. Jarosław Z, Janusz M (2014) Prony's method with reduced sampling—numerical aspects. Metrol Meas Syst 21(3):521–534. https://doi.org/10.2478/mms-2014-0044
19. Mohammad F, Javad S (2104) Transmission line fault location using hybrid wavelet-Prony method and relief algorithm. Electr Power Energy Syst 61:127–136. https://doi.org/10.1016/j.ijepes.2014.03.045
20. Jun M, Pawel J, Robert K, Carlos T, Benjamin C (2010) Joint processing of forward and backward extended Prony and weighted spectral semblance methods for robust extraction of velocity dispersion data. In: SPWLA 51st annual logging symposium, Australia, pp 1–13
21. Shuang Z, Kenneth A (2017) Forward and backward extended Prony (FBEP) method for power system small-signal stability analysis. IEEE Trans Power Syst 32(5):1–9. https://doi.org/10.1109/TPWRS.2017.2649879
22. Zoppi M, Tipaldi M, Cerbo A (2018) Cross-model verification of the electrical power subsystem in space projects. Measurement 112:473–483. https://doi.org/10.1016/j.measurement.2018.01.014
23. Pajusalu M, Rantsus R, Pelakauskas M, Leitu A (2012) Design of the electrical power system for the ESTCube-1 satellite. Latv Phys Tech Sci J 49(3):16–24. https://doi.org/10.2478/v10047-012-0014-4
24. Habbati B, Ramdani Y, Moulay F (2014) A detailed modeling of photovoltaic module using MATLAB. NRIAG J Astron Geophys 3(1):53–61. https://doi.org/10.1016/j.nrjag.2014.04.001
25. Mehrdad D, Abdelhamid R (2013) Comprehensive modulation and classification of faults and analysis their effect in dc side of photovoltaic system. Energy Power Eng 5:230–236. https://doi.org/10.4236/epe.2013.54B045
26. Arani MS, Hejazi MA (2016) The comprehensive study of electrical faults in PV arrays. Electr Comput Eng J 2016:1–10. https://doi.org/10.1155/2016/8712960
27. Ehab A, Wael A, (2017) Efficient anomaly classification for spacecraft reaction wheels. Neural Comput Appl. https://doi.org/10.1007/s00521-017-3226-y

28. Ramdas K, Donald W, Louis L (1984) A Prony method for noisy data: choosing the signal components and selecting the order in exponential signal models. IEEE Proc 72(2):230–233. https://doi.org/10.1109/PROC.1984.12849
29. Xiaoling Y, Baohua T, Jiehua D, Jinye Z, Jiaoli G. (2010) Comparative study on voice activity detection algorithm. In: IEEE international conference on electrical and control engineering Wuhan, China, pp 599–602. https://doi.org/10.1109/icece.2010.153
30. Lie L, Hong Z (2002) Content analysis for audio classification and segmentation. IEEE Trans Speech Audio Proc 10(7):504–516. https://doi.org/10.1109/tsa.2002.804546
31. Baoxiang W, Hongxia P, Wei Y (2017) A complementary approach for fault diagnosis of rolling bearing using canonical variate analysis based short-time energy feature. J Vib Control 1–16. https://doi.org/10.1177/1077546317721844 I:
32. Gareth J, Daniela W, Trevor H, Robert T (2013) An Introduction to statistical learning. Springer, New York
33. Thomas S (2007) Applied linear algebra and matrix analysis. Springer, Berlin
34. Omran EA, Murtada WA, Serageldin A (2017) Spacecraft onboard real time software architecture for fault detection and identification. In: 12th IEEE international conference on computer engineering and systems (ICCES) Cairo, pp 615–620. https://doi.org/10.1109/icces.2017.8275379
35. Jiye S, Hu W, Hong H, Yu L, Kesheng (2012) Study on modeling and diagnosis of the satellite power system. In: IEEE international conference on quality, reliability, risk, maintenance, and safety engineering (ICQR2MSE) China, pp 607–611. https://doi.org/10.1109/icqr2mse.2012.6246307
36. Matthew D, Anibal B, Indranil R (2012) Qualitative event-based diagnosis with possible conflicts applied to spacecraft power distribution systems. IFAC Proc 45(20):265–270. https://doi.org/10.3182/20120829-3-MX-2028.00084
37. Rui Q, Wei Q, Xiaochen W, Lingwei Y, Hongbo H (2014) Health status management of spacecraft power system based on hidden markov model. In: IEEE international conference on prognostics and system health management (PHM), China, pp 673–677. https://doi.org/10.1109/phm.2014.6988258
38. Ole J, Scott P, Tolga K (2009) Developing large-scale bayesian networks by composition: fault diagnosis of electrical power systems in aircraft and spacecraft. In: IJCAI-09 workshop on self and autonomous systems: reasoning and integration challenges (SAS-09), USA, pp 59–66
39. Yi L, Ke L, Yong H, Jun W, Shimin S, Yi Sun (2014) Spacecraft electrical characteristics identification study based on offline FCM clustering and online SVM classifier. In: International conferrence on multisensor fusion and information integration for intelligent systems (MFI) China, pp 1–4. https://doi.org/10.1109/mfi.2014.6997666
40. Ke L, Yalei W, Shimin S, Yi S, Jun W, Yang L (2016) A novel method for spacecraft electrical fault detection based on FCM clustering and WPSVM classification with PCA feature extraction. Proc Inst Mech Eng Aerosp Eng J 231(1):98–108. https://doi.org/10.1177/0954410016638874
41. Myeongsu K, Jong K (2013) Singular value decomposition based feature extraction approaches for classifying faults of induction motors. Mech Syst Signal Proc 41:348–356. https://doi.org/10.1016/j.ymssp.2013.08.002
42. Dawei P, Datong L, Jun Z, Guoyong Z (2015) Anomaly detection for satellite power subsystem with associated rules based on kernel principal component analysis KPCA. Microelectron Reliab 55(9–10):2082–2086. https://doi.org/10.1016/j.microrel.2015.07.010
43. Yi L, Ke L, Shimin S, Yi S, Yong H, Jun W (2014) The research of spacecraft electrical characteristics identification and diagnosis using PCA feature extraction. In: 12th IEEE international conference on signal processing (ICSP) China, pp 1413–141. https://doi.org/10.1109/icosp.2014.7015232
44. Harrou F, Taghezouit B, Sun Y (2019) Improved KNN-based monitoring schemes for detecting faults in PV systems. IEEE J Photovolt 2019:1–11. https://doi.org/10.1109/JPHOTOV.2019.2896652
45. Ahmadi M, Samet H, Ghanbari T (2019) Kalman filter–based approach for detection of series arc fault in photovoltaic systems. Int Trans Electr Eng Syst 2019:1–21. https://doi.org/10.1002/2050-7038.2823